Transient Development of Backward Stimulated Raman and Brillouin Scattering on a Picosecond Time Scale Measured by Subpicosecond Thomson Diagnostic

C. Rousseaux, L. Gremillet, M. Casanova, P. Loiseau, and M. Rabec Le Gloahec
Commissariat à l'Energie Atomique, Direction d'Ile de France, 91680 Bruyères-le-Châtel, France

S. D. Baton and F. Amiranoff
LULI, UMR 7605, CNRS-CEA-École Polytechnique-Université Paris VI, École Polytechnique, 91128 Palaiseau, France

J. C. Adam and A. Héron
Centre de Physique Théorique, CNRS, École Polytechnique, 91128 Palaiseau Cedex, France
(Received 22 December 2005; published 7 July 2006)

The excitation and the relaxation of the plasma waves and ion acoustic waves (IAW), respectively, driven by stimulated Raman (SRS) and Brillouin (SBS) backscatterings have been experimentally investigated with short-pulse lasers. The spectra have been obtained with a 0.3 ps time resolution. It is shown that SRS develops before SBS and suddenly decays around the peak of the pump, as the IAW reaches saturation. On this short time scale, electron kinetic effects play a major role for SRS saturation, contrary to ion dynamics. These results are supported by particle-in-cell simulations.

DOI: 10.1103/PhysRevLett.97.015001 PACS numbers: 52.38.−r, 52.35.Fp, 52.35.Mw, 52.70.Nc

Acquiring a quantitative prediction capability for the saturation of parametric instabilities driven in the laser-plasma interaction presents one of the most challenging roadblocks to achieving the laser inertial confinement fusion (ICF) programs currently under way [1]. Indeed, laser-plasma instabilities (LPI) such as stimulated Brillouin backscattering (B-SBS) or stimulated Raman backscattering (B-SRS) [2] can redistribute a significant part of the incident light beams when traveling through the millimeter-size, homogeneous plasmas filling an indirect-drive hohlraum target. Here, SBS and SRS refer, respectively, to the laser-plasma instabilities whereby the laser pump resonantly scatters off an ion acoustic wave (IAW) or an electron plasma wave (EPW). In addition to the electron preheat due to the damping of the driven EPW, the compression efficiency of the pellet and the energy gain could be severely degraded.

One major difficulty impeding a realistic modeling of LPI experiments has long been the interplay between the waves generated by primary and secondary instabilities during the interaction [2]. As a result, Thomson scattering-based diagnostics are often employed to characterize both the hydrodynamic state of the plasma and the features of the instability-driven electrostatic waves with unprecedented spatial and wave number resolutions [3–5]. Yet, besides wave-coupling processes, an accurate description of the interaction physics often requires kinetic effects to be addressed. The nonlinear Landau damping of the driven EPW and IAW leads to non-Maxwellian velocity distributions likely, in turn, to noticeably alter the transport and wave damping coefficients [6]. In this respect, Kline *et al.* [7] have recently found a transition from fluid to kinetic effects above $k\lambda_D \approx 0.29$ (where k is the wave number of the most unstable SRS-driven EPW and λ_D is the Debye length). A further complication stems from the short growth time of the plasma instabilities whose saturated regime is reached within a few picoseconds, to be compared with both the typical nanosecond pulse duration and the ~30 ps time resolution of a streak camera. Using low intensity CO_2 lasers, the SBS growth rate was directly measured [4], but the time resolution was not accurate enough to diagnose electron time-scale phenomena such as SRS. Thus, the experimental data obtained with standard lasers can be analyzed only in conjunction with saturation models in *asymptotic regimes*, averaged over a few tens of picoseconds. By contrast, subpicosecond-time-resolved diagnostics coupled with short-pulse interaction can be directly confronted with simulation codes solving the full set of Vlasov-Maxwell equations, hence self-consistently accounting for fast non-Maxwellian effects [8]. A further advantage provided by short pulses is that the instabilities can be identified from their onset, i.e., from a plasma with known hydrodynamic conditions near the local thermodynamic equilibrium. The linear phase of development can then be diagnosed up to the first steps of saturation [9].

This Letter reports on the first experimental, simultaneous measurements of the transient development of EPW and IAW driven by B-SRS and B-SBS with subpicosecond resolution. These results have been favorably compared with 1D and 2D particle-in-cell (PIC) simulations. In particular, both calculations and measurements suggest that the ion dynamics does not contribute much to the SRS saturation in our experimental, picosecond time-scale conditions. The interaction physics seems, in our case, to be dominated by kinetic effects.

The experiment has been performed at LULI laboratory using the 100-TW laser facility. The setup is shown in Fig. 1. The plasma is preformed by firing a random phase plate (RPP)-smoothed, $f/7$, 1.059 μm beam onto a He gas

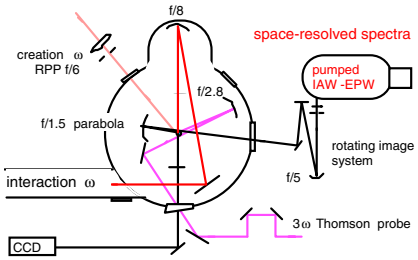

FIG. 1 (color online). Setup of the experiment.

puff, 1 mm in diameter. Focused within a 100 μm $\times$ 500 μm spot, this 550 ps FWHM beam with a 10^{14} W/cm^2 mean intensity leads to the full ionization of the gas. The main interaction beam is then fired along the large dimension of the plasma, at an angle of 35° with respect to the heating beam and 0.2 ns after its maximum. This beam has a wavelength centered at 1.059 μm and a duration of 1.5 ps FWHM. It is focused by a $f/8$ off-axis parabola, producing a 15 μm diameter focal spot (containing 70% of the energy). The focal depth was measured to be larger than 500 μm. In these experimental conditions, 2D hydrodynamic simulations performed by the code FCI2 [10] indicate a Gaussian electron density peaking at 4×10^{19} cm^{-3} (i.e., $0.04n_c$, where n_c is the critical density at ω) and electron (ion) temperatures just before the picosecond interaction close to 300 eV (50 eV). The main beam impinges upon the edge of the plasma where the local electron density scale length is calculated to be 200 μm.

The main diagnostic consists of Thomson scattering off the B-SRS–driven EPW and the B-SBS–driven IAW. A small energy fraction split from the main chirped pulse, independently time compressed and frequency tripled, yields a 2 mJ Thomson probe with a 0.3 ps FWHM and a spectral width of typically 1.2 nm. Absolute synchronization within 1 ps between the maxima of the probe and the main pulse is ensured by means of a shadowgraphy technique: the probe diagnoses the onset of the breakdown of the He gas caused by the main pulse. The time delay between these two pulses is completely immune from jitter and can be adjusted from shot to shot with a precision better than 0.15 ps. The $f/2.8$ probe is focused into the interaction region at an angle of 63° with respect to the direction of the pump and within a 300-μm-long rectangular volume. We stress that, contrary to standard Thomson experiments, the duration of the probe is shorter than the period of the strongly driven IAW ($2\pi/\omega_{\mathrm{IAW}} \sim$ 1 ps at $\sim 10^{17}$ W/cm^2), which prevents the latter from being spectrally resolved. The scattered light is collected at 100° with respect to the pump direction ($f/1.5$ aperture) and imaged with an achromatic optical array onto the slit of an imaging spectrometer, coupled to a 4-ns-gated, 16 bits UV CCD. With this large aperture diagnostic, the IAWs and the EPWs parallel (within a few degrees) to the pump are detected in the range of k_0–$2.8k_0$, where k_0 is the vacuum wave number of the pump. Each measurement provides a 0.3 ps FWHM "snapshot" of the spatially resolved spectrum along the direction of the main pulse (with a resolution better than 100 μm). The time history of the driven waves is obtained by varying the time delay between the probe and the main pulse from shot to shot. The 1.5 nm spectral resolution is determined by both the probe bandwidth and the slit of the spectrometer.

Figures 2 and 3 present a typical time history of the SBS-IAW and SRS-EPW as measured at an intensity of

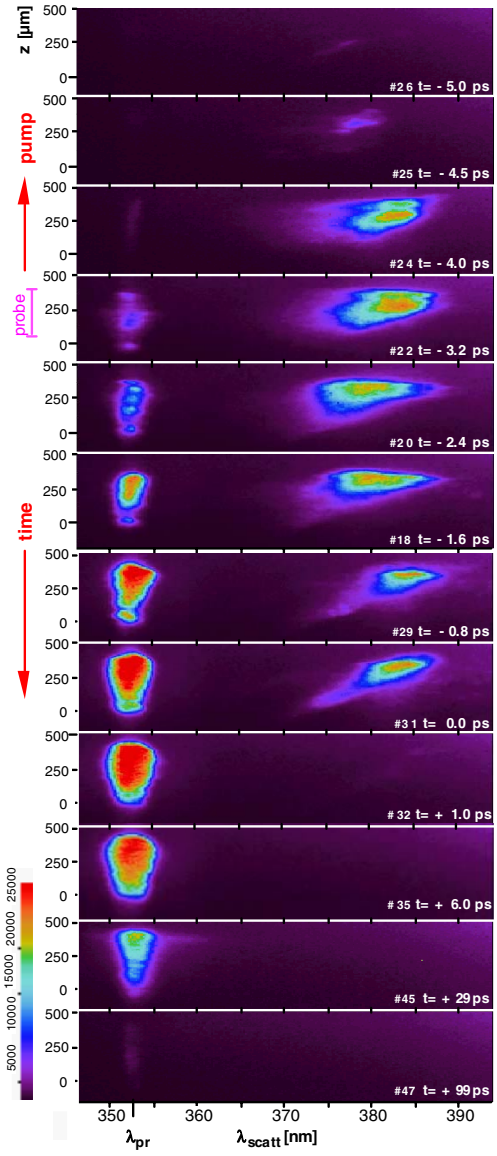

FIG. 2 (color online). Temporal evolution of the IAW and EPW driven by the 1.5 ps laser pulse ($I = 9 \times 10^{17}$ W/cm^2). The spectra are space resolved, identically filtered, and share the same linear color scale. The pump propagates along z. The IAWs are measured near the probe wavelength λ_{pr}, while the EPWs can be found around 385 nm. The large dynamic range of the CCD explains the somewhat weak contrast and the apparent saturation of the IAW spectra.

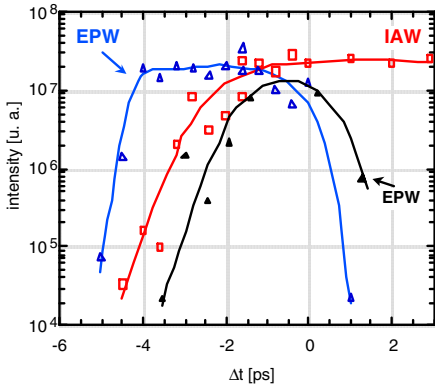

FIG. 3 (color online). Temporal evolution of scattered intensities off IAWs (red open squares) and EPWs (blue open triangles) as measured from Fig. 2. The black line (black solid triangles) corresponds to the EPW signal obtained at a lower intensity (7×10^{15} W/cm^2), for which the IAW signal remains below the detection level. Note that the EPWs are quickly damped near the peak of the pulse, regardless of the mean laser intensity.

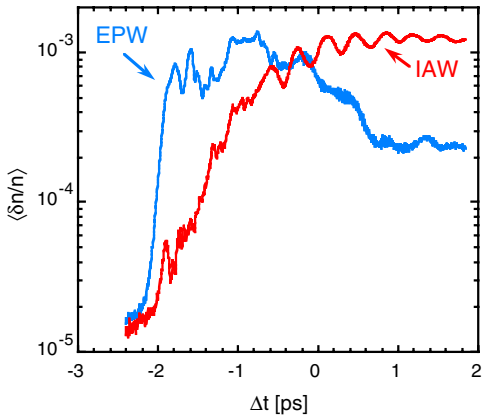

FIG. 4 (color online). Mean relative amplitude $\langle \delta n/n \rangle$ as a function of time of the driven EPW with $k = (1.725 \pm 0.01)k_0$ and IAW with $k = (1.96 \pm 0.01)k_0$, as calculated by the 2D PIC code. The origin $t = 0$ corresponds to the pulse maximum reaching the middle of the box.

9×10^{17} W/cm^2. The observed scenario has been obtained repeatedly in various interaction conditions, i.e., at different plasma densities and over a large intensity range (from 10^{16} W/cm^2 to 10^{18} W/cm^2). Figure 2 shows the time-resolved spectra, whereas Fig. 3 plots the scattered intensity off the driven waves as a function of time. The EPW measurement at low intensity (7×10^{15} W/cm^2) will be discussed later. The time resolution is 0.3 ps, and $t = 0$ refers to the peak of the main pulse. In Fig. 2, we observe that the SRS-driven EPWs are excited first, early in the rising part of the pulse. They reach their saturation level in $\sim$1 ps. The appearance of IAWs coincides with EPW saturation: they grow more slowly and mainly in the same area. Spatial modulations of the IAWs along the propagation of the pulse are clearly visible during their growth. They develop over $\sim$3 ps and reach saturation near the top of the laser pulse. The EPWs and IAWs coexist until this time, beyond which the former suddenly vanish. During the falling part of the pulse, the IAWs are left alone in the plasma and slowly damped, being detectable up to 100 ps after the pump. The different spectral widths shown in Fig. 2 are rather large. Regarding the EPWs, several sources for broadening are possible, such as B-SRS driven in the strong field regime, plasma inhomogeneity, trapping effects, or relativistic effects. However, it can be noticed that the EPW spectrum becomes broad early ($\sim$10 nm), at a time where the laser intensity is still low, thus indicating that the B-SRS growth rate may be not the main cause of this width. Moreover, experiments performed at low intensities (7×10^{15} W/cm^2) have shown narrow spectra ($\leq$2 nm) during the first 1.5–2 ps and spectral broadening ($\sim$10 nm) near the peak of the pump. This may also rule out the preponderant role of the growth rate. On the other hand, the IAW's spectral width significantly exceeds the one calculated at high intensity in the strong decay regime of SBS, being of the order or less than the spectral resolution (1.5 nm). This feature may be attributed to a pronounced modification of the velocity distribution functions of both ions and electrons as predicted by the PIC simulations presented below. Yet, a quantitative analysis of how such deformations may affect the measured spectra clearly exceeds the scope of this Letter.

The obtained data also allow direct measurement of the IAW decay time provided it is longer than the laser falling time. We thus estimated the damping rate in He to be $\nu_{\mathrm{IAW}} \sim 1.5$–$3 \times 10^{10}$ s^{-1} ($\nu_{\mathrm{IAW}}/\omega_{\mathrm{IAW}} \sim 10^{-2}$), which is surprisingly comparable to that obtained with classical Landau damping and $ZT_e/T_i \gg 1$. Again, the influence of altered distribution functions is not clear, and future work will address this damping in other gases, including hydrocarbon gases.

In the presence of a pump with a steep rise time (as is the case with short pulses), this chronology agrees with the linear theory predicting that the instability characterized by the largest growth rate (B-SRS) sets in first. A far more complete modeling is provided by PIC simulations. In the one-dimensional case considered by Estabrook *et al.* [11], the laser pulse propagates through a $0.05n_c$ homogeneous plasma with an intensity $I\lambda^2 = 2 \times 10^{15}$ W μm^2/cm^2. B-SRS then exhibits an intense burst before being quenched once the IAW-SBS becomes significant. B-SBS is seen to prevail later on, while other phenomena start developing, such as pump depletion, secondary instabilities, and nonthermal electron heating.

We obtained similar results with our 1D PIC code but based our analysis on 2D simulations which no longer neglect potentially relevant processes, such as side-scattering instabilities, density depletion, or self-focusing. In these simulations, the plasma consists of a 450-μm-long, 220-μm-wide slab with a density $n/n_c =$

0.04 and an initial temperature of 500 eV. Boundary conditions for the electromagnetic fields are open-ended along the laser axis and periodic in the transverse direction. Energetic particles reaching the end of the slab are replaced by cold ones. Thirty cells are used per wavelength, each containing 10 particles yielding a total number of 10^9 particles per species. The 1.6 ps FWHM Gaussian laser pulse starting 2.4 ps before maximum is focused in the middle of the plasma within a 10 μm focal spot at a maximum intensity $I\lambda^2$ around 10^{17} W μm^2/cm^2. The simulation is carried on up to 5 ps. In the following, we restrict the analysis of the data to the time history of the instabilities.

The evolution of the mean values of the electron density variation $\delta n/n$ filtered in the vicinity of $1.72k_0$ (for B-SRS) and $1.96k_0$ (for B-SBS), averaged over a 200-μm-long, 30-mm-wide plasma volume, are plotted in Fig. 4. Here k_0 denotes the interaction pulse wave number in vacuum and the time $t = 0$ refers to the pulse peak as seen in the middle of the slab.

Quick development of B-SRS, preceding a more slowly growing B-SBS, is clearly evidenced. For comparison, at $I\lambda^2 = 10^{17}$ W μm^2/cm^2, the homogeneous growth rate of B-SRS [B-SBS] in the modified decay regime is about $(10\ \text{fs})^{-1}$ [$(90\ \text{fs})^{-1}$], as calculated in the kinetic, nonrelativistic regime [12] or in the cold relativistic regime [13]. The earlier onset of the amplified electrostatic waves detected in the experiment may point to a pulse shape not exactly Gaussian, with a rise time longer than expected. The B-SRS quenching occurring near the top of the pulse agrees remarkably well with the experiment. Since the decay of SRS observed in both experiment (Fig. 2) and simulations (Fig. 4) coincides with the pump maximum and a high IAW level, we are compelled to gauge the role of ion dynamics. First, a measurement made at low intensity (7×10^{15} W/cm^2, Fig. 3) shows a similar EPW evolution to that obtained previously, but without detectable evidence of IAWs. Second, 1D-PIC simulations performed with or without mobile ions exhibit mostly unchanged time histories of SRS. They indicate that, within the picosecond time scale of our experiment, nonlinear kinetic effects such as trapping and the associated deformation of the electron distribution are the main cause for SRS saturation.

In summary, the concomitant development of the electrostatic waves driven by B-SRS and B-SBS has been experimentally diagnosed with an unprecedented subpicosecond time resolution. Within such a short time scale, measurements compare remarkably well with PIC calculations. Trapping effects seem to be the likely cause for the sudden disruption of B-SRS at a time where the pump is still intense, as ion dynamics do not have enough time to play a major role. These results can help us understand the saturation processes of parametric instabilities occurring in large-scale plasmas, a topic of critical importance for the ICF program.

We acknowledge the beneficial support from the LULI technical staff during these experiments and O. Bernard (Andor Technology) for lending us the gated UV CCD. Part of the work was supported by Grant No. E1127 from Région d'Ile de France. Simulations were carried out at IDRIS, Computing Center of CNRS (France).

[1] J. Lindl, Phys. Plasmas **2**, 3933 (1995); J. D. Lindl, *Inertial Confinement Fusion: The Quest for Ignition and Energy Gain Using Indirect Drive* (Springer-Verlag, New York, 1998).

[2] D. Pesme, *La Fusion Thermonucléaire Inertielle par Laser*, edited by R. Dautray and J. P. Watteau (Eyrolles, Paris, 1993), Pt. 1, Vol. 1, Chap. II; W. L. Kruer, *The Physics of Laser Plasma Interactions* (Addison-Wesley, New York, 1988); H. A. Baldis, E. M. Campbell, and W. L. Kruer, *Handbook of Plasma Physics*, edited by M. N. Rosenbluth and R. Z. Sagdeev, Physics of Laser Plasma Vol. 3, edited by A. M. Rubenchik and S. Witkowski (Elsevier, New York, 1991).

[3] J. Sheffield, *Plasma Scattering of Electromagnetic Radiation* (Academic, New York, 1975).

[4] R. Giles and A. A. Offenberger, Phys. Rev. Lett. **50**, 421 (1983); J. E. Bernard and J. Meyer, Phys. Rev. Lett. **55**, 79 (1985).

[5] J. E. Bernard *et al.*, Phys. Rev. A **39**, 2549 (1989); C. J. Walsh, D. M. Villeneuve, and H. A. Baldis, Phys. Rev. Lett. **53**, 1445 (1984); D. M. Villeneuve, H. A. Baldis, and J. E. Bernard, Phys. Rev. Lett. **59**, 1585 (1987); D. S. Montgomery *et al.*, Phys. Plasmas **9**, 2311 (2002); D. H. Froula *et al.*, Phys. Rev. Lett. **93**, 035001 (2004).

[6] B. B. Afeyan *et al.*, Phys. Rev. Lett. **80**, 2322 (1998); D. A. Russell, D. F. DuBois, and H. A. Rose, Phys. Plasmas **6**, 1294 (1999); H. X. Vu, D. F. DuBois, and B. Bezzerides, Phys. Plasmas **9**, 1745 (2002).

[7] J. L. Kline *et al.*, Phys. Rev. Lett. **94**, 175003 (2005).

[8] C. Rousseaux *et al.*, Phys. Plasmas **9**, 4261 (2002).

[9] C. Rousseaux *et al.*, Phys. Rev. Lett. **74**, 4655 (1995).

[10] G. Schurtz, *La Fusion Thermonucléaire Inertielle par Laser*, edited by R. Dautray and J. P. Watteau (Eyrolles, Paris, 1993), Pt. 3, Vol. 2, p. 1117.

[11] K. G. Estabrook, W. L. Kruer, and M. G. Haines, Phys. Fluids B **1**, 1282 (1989).

[12] D. W. Forslund *et al.*, Phys. Fluids **18**, 1002 (1975).

[13] S. Guérin, Phys. Plasmas **2**, 2807 (1995).